

The Global Schmidt Law in Star Forming Galaxies ¹

Robert C. Kennicutt, Jr.

Steward Observatory, University of Arizona, Tucson, AZ 85721

ABSTRACT

Measurements of $H\alpha$, HI, and CO distributions in 61 normal spiral galaxies are combined with published far-infrared and CO observations of 36 infrared-selected starburst galaxies, in order to study the form of the global star formation law, over the full range of gas densities and star formation rates (SFRs) observed in galaxies. The disk-averaged SFRs and gas densities for the combined sample are well represented by a Schmidt law with index $N = 1.4 \pm 0.15$. The Schmidt law provides a surprisingly tight parametrization of the global star formation law, extending over several orders of magnitude in SFR and gas density. An alternative formulation of the star formation law, in which the SFR is presumed to scale with the ratio of the gas density to the average orbital timescale, also fits the data very well. Both descriptions provide potentially useful “recipes” for modelling the SFR in numerical simulations of galaxy formation and evolution.

Subject headings: galaxies: evolution — galaxies: ISM — galaxies: spiral — galaxies: starburst — stars: formation

1. INTRODUCTION

A key ingredient in the understanding and modelling of galaxy evolution is the relationship between the large-scale star formation rate (SFR) and the physical conditions in the interstellar medium (ISM). Most current galaxy formation and evolution models treat star formation using simple ad hoc parametrizations, and our limited understanding of the actual form and nature of the SFR-ISM interaction remains as one of the major limitations in these models (e.g., Navarro & Steinmetz 1997). Measurements of the star

¹Visiting Astronomer, Kitt Peak National Observatory, National Optical Astronomical Observatories, which are operated by the Association of Universities for Research in Astronomy, Inc., under contract with the National Science Foundation.

formation law in nearby galaxies can address this problem in two important respects, by providing empirical “recipes” that can be incorporated into analytical models and numerical simulations, and by providing clues to the physical mechanisms that underlie the observed correlations.

The most widely applied star formation law remains the simple gas density power law introduced by Schmidt (1959), which for external galaxies is usually expressed in terms of the observable surface densities of gas and star formation:

$$\Sigma_{SFR} = A \Sigma_{gas}^N \quad (1)$$

The validity of the Schmidt law has been tested in dozens of empirical studies, with most measured values of N falling in the range 1 – 2, depending on the tracers used and the linear scales considered (Kennicutt 1997). On large scales the star formation law shows a more complex character, with a Schmidt law at high gas densities, and a sharp decline in the SFR below a critical threshold density (Kennicutt 1989, hereafter K89). These thresholds appear to be associated with large-scale gravitational stability thresholds for massive cloud formation (e.g., Quirk 1972; Fall & Efstathiou 1980; K89). At high gas densities, well above the stability threshold, the form of the Schmidt law appears to be remarkably consistent from galaxy to galaxy, both in terms of its slope ($N \sim 1.3 - 1.5$) and the absolute SFR efficiency (the coefficient A in eq. [1]). Studies of this kind offer the beginnings of a quantitative, physical prescription for the SFR that can be incorporated into galaxy formation and evolution models.

This is the first of two papers which reinvestigate the form and physical nature of the star formation law, over a much larger range of galaxy types and gas densities than was possible previously. Paper II (Martin & Kennicutt 1998) uses new H α CCD imaging of an HI and CO selected sample of spiral galaxies to quantify the behavior of the star formation law within individual galaxies, and to test several models for the star formation law. This paper is concerned with the behavior of the star formation law on global scales, averaged over the entire star forming disk. Such global laws, which treat galaxies in a single-zone approximation, provide less physical insight into the star formation process itself, but they provide very useful parametrizations (recipes) for galaxy evolution modelling.

Earlier work has shown that the global, disk-averaged star formation law is reasonably well represented by a Schmidt law (K89; Buat, Deharveng, & Donas 1989; Buat 1992; Boselli 1994; Deharveng et al. 1994). However these analyses have been hampered by small samples and by the small range of gas densities represented in those samples. In this paper we use newly available HI, CO, and H α data to more than double the sample over previous studies, and fully cover the range of mean gas densities found in disks. We

combine these data with published CO, Br γ , and far-infrared (FIR) measurements of luminous starburst galaxies, to investigate the nature of the Schmidt law in higher density environments, thereby extending the total density range probed to nearly five orders of magnitude. Our main goal is to test whether the millionfold range in observed SFRs, extending from quiescent gas-poor disks to nuclear starbursts, can be understood within a common empirical and physical framework.

2. DATA

To investigate the global star formation law in normal disks, we searched the literature for normal galaxies with well-sampled HI and CO measurements, and for which H α imaging or photometry are available. Our analysis of this sample closely follows that described in K89. To investigate the star formation law at higher densities, we compiled published CO maps, FIR photometry, and Br γ emission-line measurements for a sample of infrared-selected starburst galaxies. Each data set is discussed separately below.

2.1. Normal Disks

Previous studies of the disk-averaged star formation law have shown that the global SFR correlates most strongly with the total (atomic + molecular) gas density (e.g., Kenney & Young 1988; K89; Buat 1992; Boselli 1994). Consequently our primary data set consists of normal spirals for which spatially-resolved HI, CO, and H α data are available. A master list of candidate galaxies was compiled from the FCRAO CO survey (Young et al. 1989; 1995), supplemented by the CO survey of Sage (1993). Within these samples, we identified 61 galaxies which also have published HI maps, H α photometry, and inclinations less than 75° (to avoid severe extinction problems in edge-on systems). Total HI masses based on single-dish measurements are available for another 150 galaxies, but those data are unsuitable for the current application, because much of the HI is located well outside of the star forming disks, and it is essential to correlate the SFR and gas densities over the same physical region. However we do use some of these additional galaxies in §3.1 to examine the form of the SFR *vs* HI Schmidt law.

Table 1 lists the 61 galaxies in the sample, the relevant surface densities, and references, as described below. When considering the sample properties as a whole the main selection criterion was availability of CO and HI maps, so the galaxies should comprise a virtually unbiased set in terms of star formation properties. Approximately 40% of the galaxies are

members of the Virgo cluster, selected from the CO survey of Kenney & Young (1988) and the HI survey of Warmels (1988), and this sample contains most of the luminous spirals in the cluster core. The field galaxy subsample is more heterogeneous, and is significantly biased toward galaxies of Hubble type Sb and later, but it is unlikely that this selection biases the form of the star formation law.

HI surface densities were taken mainly from the compilations of Warmels (1988), Broeils & van Woerden (1994), and Rhee & van Albada (1995), supplemented by individual measurements of a few galaxies (Table 1). The mean HI surface densities, averaged within the optical radius of the disk, were derived from the surface density profiles given in those papers or the references therein. The disk radii are the corrected isophotal radii as given in the RC2 catalog (de Vaucouleurs, de Vaucouleurs, & Corwin 1976). The mean densities used here differ from those that are often tabulated in the original papers, the latter usually being averaged within the inner *half* of the optical disk.

Total molecular hydrogen masses were taken from the Young et al. (1989; 1995) and Sage (1993) surveys, and converted when needed to a common CO/H₂ conversion factor: $N(H_2) = 2.8 \times 10^{20} I_{CO} \text{ cm}^{-2} \text{ (K km s}^{-1}\text{)}$. The mean H₂ surface densities were then determined, by averaging within the radii listed in Table 1. These average densities are meaningful only if the CO emission is confined to the optical disk, and the measurements extend to a substantial fraction of optical radius. Galaxies which were sampled to less than half of the optical radius were not included in our sample.

Integrated SFRs were derived from measurements of the H α emission-line flux, following the method described in Kennicutt (1983). Most of the H α fluxes were taken from the surveys of Kennicutt & Kent (1983), Romanishin (1990), and Young et al. (1996). Those data were supplemented with new calibrated H α CCD images obtained with a focal reducer camera on the Steward Observatory 2.3 m Bok telescope, and with the 0.9 m and Burrell Schmidt telescopes at Kitt Peak National Observatory. Details of these observations are given in Paper II. The H α fluxes were corrected as needed for foreground extinction and [NII] emission, following the prescriptions in Kennicutt (1983). The original H α fluxes of Kennicutt & Kent (1983) have been corrected upwards by a factor of 1.16 to place them on a consistent zeropoint with more recent measurements (Romanishin 1990; Kennicutt 1992).

The H α luminosities were then converted to total SFRs, using the updated calibration of Kennicutt, Tamblyn, & Congdon (1994):

$$SFR (M_{\odot} \text{ yr}^{-1}) = \frac{L(H\alpha)}{1.26 \times 10^{41} \text{ ergs s}^{-1}} \quad (2)$$

The H α luminosities used in equation (2) were corrected for internal extinction by 1.1

mag (factor 2.8), based on a comparison of free-free radio fluxes and $H\alpha$ fluxes of galaxies by Kennicutt (1983). The actual extinction varies within the sample, of course, which introduces significant scatter in the observed star formation law, as discussed later. While it would be much better to apply individual extinction corrections to each galaxy, determining the reddening or extinction from integrated spectra is problematic (Kennicutt 1992), and would introduce uncertainties that are larger than the single average correction. It may be possible in the future to derive improved estimates of the extinction and SFR using measurements of near-infrared Brackett or Paschen recombination lines, but such data are not currently available.

The IMF used in this conversion is a Salpeter function ($dN(m)/dm = -2.35$) over $m = 0.1 - 100 M_{\odot}$. The Salpeter IMF was adopted in order to be consistent with the infrared-derived SFRs in the next section. Adopting the extended Miller-Scalo function used in Kennicutt (1983) would produce nearly identical SFRs (only 8% lower). Galaxy distances from Young et al. (1989) were used in this intermediate calculation, but the distances are irrelevant for most of this paper, because the Schmidt law is analyzed in terms of distance-independent surface densities.

Finally, the mean SFR surface density (units $M_{\odot} \text{ yr}^{-1} \text{ kpc}^{-2}$) was derived for each galaxy, by dividing the total SFR from equation (2) by the deprojected area within the corrected RC2 radius. Through the remainder of this paper, we shall refer to this SFR per unit area as the “SFR density”. In most galaxies the RC2 radius coincides approximately with the edge of the main $H\alpha$ -emitting disk (K89), so the SFR density as measured here corresponds roughly to the mean SFR per unit area within the active star forming disk. The derived SFR surface densities are listed in Table 1. The observed $H\alpha$ surface densities (uncorrected for extinction) can be derived from Table 1 by the simple relation: $\log \Sigma_{H\alpha} = \log \Sigma_{SFR} + 34.65$, where $\Sigma_{H\alpha}$ is expressed in units of $\text{ergs sec}^{-1} \text{ pc}^{-2}$. This conversion may be useful for readers who may wish to apply a different SFR calibration to the $H\alpha$ data compiled here.

2.2. Infrared-Selected Starburst Galaxies

The mean gas densities of the normal spiral disks in our sample lie within a relatively narrow range, from 2 to 50 $M_{\odot} \text{ pc}^{-2}$, and this seriously limits the dynamic range over which the behavior of the Schmidt law can be evaluated. The density range can be extended to $\sim 100 M_{\odot} \text{ pc}^{-2}$ by analyzing spatially-resolved measurements of individual disks (Paper II), but above these densities $H\alpha$ measurements become unreliable for determining the SFR. For a typical gas-to-dust ratio found in nearby galaxies, the visual extinction reaches 1 mag

for column densities $N_H \sim 2 - 4 \times 10^{21} \text{ cm}^{-2}$, or $\Sigma_H \sim 15 - 30 \text{ M}_\odot \text{ pc}^{-2}$ (e.g., Bohlin, Savage, & Drake 1978; Caplan & Deharveng 1986). Hence one expects the extinction at $\text{H}\alpha$ to become problematic for regions with mean gas surface densities above $50 - 100 \text{ M}_\odot \text{ pc}^{-2}$. If we wish to study the nature of the star formation law in these dense regions, a star formation diagnostic other than $\text{H}\alpha$ must be used.

Large-scale star formation at much higher densities is commonly found in the centers of normal galaxies, and particularly in luminous infrared starburst galaxies. In order to analyze the star formation law in this regime, we searched the literature for high-resolution CO and infrared measurements of starburst galaxies. Since the starbursts are often concentrated in compact circumnuclear disks (e.g., Scoville et al. 1994; Sanders & Mirabel 1996; Smith & Harvey 1996), high-resolution data are required in order to accurately determine the linear sizes of the starburst regions and the corresponding surface densities. Our sample comprises 36 galaxies with high-resolution CO data, most based on aperture synthesis mapping, and for which infrared measurements of the same region are available. The sample ranges from low-level nuclear starbursts in normal and peculiar galaxies such as NGC 253, IC 342, Maffei 2, and M82 ($L_{FIR} \sim 10^8 - 10^{10} L_\odot$) to ultraluminous starburst galaxies with $L_{FIR} > 10^{12} L_\odot$ (e.g., Arp 220). Care was taken to select objects in which the dust heating is dominated by a starburst, as determined from optical spectra spectra (e.g., Armus, Heckman, & Miley 1989; Veilleux et al. 1995) and/or mid-infrared spectroscopy (e.g., Lutz et al. 1996). Objects with evidence for a strong AGN component were excluded (e.g., NGC 1068, NGC 7469, Mrk 231, Mrk 273).

Total molecular gas masses in the starburst disks were derived from the CO flux and distance, using the same CO/ H_2 conversion factor as for the normal galaxies. The validity of a constant conversion factor is highly questionable (e.g., Wild et al. 1992; Downes, Solomon, & Radford 1993; Aalto et al. 1994; Solomon et al. 1997), and we have adopted a uniform conversion factor strictly for the sake of simplicity. The impact of adopting a different conversion factor will be discussed later. The mean molecular surface densities were then derived, averaged within the radius of the central molecular disk as determined from the CO maps.

High-resolution HI observations are only available for a few of these galaxies, and in those cases the atomic fraction in the circumnuclear region is small, of order a few percent or less (e.g., Garcia-Barreto 1991; Downes et al. 1996; Sanders & Mirabel 1996). This is not surprising given the very high column densities found in these regions. Consequently we have ignored the HI component and approximate the molecular mass as the total gas mass in the starburst region. Table 2 lists the galaxies in the sample, the radii of the disks, and their mean molecular surface densities.

The SFRs for the starbursts were derived from measurements of their FIR luminosities. These were taken from a variety of sources, as listed in Table 2. For about half of the sample, high-resolution maps at mid-infrared wavelengths are available, and when combined with IRAS fluxes for the galaxies as a whole they provide an accurate estimate of the FIR luminosity in the central starbursts themselves (Telesco, Dressel, & Wolstencroft 1993; Smith & Harvey 1996). For the other galaxies the FIR luminosity of the starburst was derived from a combination of IRAS photometry and groundbased aperture photometry at 10–20 μm , or from the IRAS fluxes alone, in cases where most of the total FIR emission appears to originate in the central starburst. SFRs for three of the galaxies were derived from a combination of $\text{Br}\gamma$ and infrared photometry, as noted in Table 2.

In normal disk galaxies the relationship between the FIR luminosity and the SFR is complex, because stars with a variety of ages can contribute to the dust heating, and only a fraction of the bolometric luminosity of the young stellar population is absorbed by dust (e.g., Lonsdale & Helou 1987; Walterbos & Greenawalt 1996). However in the starbursts studied here, the physical coupling between the SFR and the IR luminosity is much more direct. Young stars dominate the radiation field that heats the dust, and the dust optical depths are so large that almost all of the bolometric luminosity of the starburst is reradiated in the infrared. This makes it possible to derive a reasonable quantitative measure of the SFR from the FIR luminosity.

Our calibration of the $\text{SFR}/L_{\text{FIR}}$ conversion is based on the starburst synthesis models of Leitherer & Heckman (1995). Their models trace the temporal evolution of the bolometric luminosity for a fixed SFR, metal abundance, and IMF. We computed the SFR calibration using their “continuous star formation” models, in which the SFR is presumed to remain constant over the lifetime of the burst. The models show that the $L_{\text{bol}}/\text{SFR}$ ratio evolves relatively slowly between ages of 10 and 100 Myr, the relevant range for most of these starbursts (e.g., Bernlöhr 1993; Engelbracht 1997). Alternatively one can derive the conversion using a “instantaneous burst” approximation, where it is assumed that star formation has ceased, but the calibration is sensitive to the presumed burst age and the (questionable) assumption of an instantaneous burst. Adopting the mean luminosity for 10–100 Myr continuous bursts, solar abundances, the Salpeter IMF described earlier, and assuming that the dust reradiates all of the bolometric luminosity yields:

$$\frac{\text{SFR}}{1 \text{ M}_{\odot} \text{ yr}^{-1}} = \frac{L_{\text{FIR}}}{2.2 \times 10^{43} \text{ ergs s}^{-1}} = \frac{L_{\text{FIR}}}{5.8 \times 10^9 L_{\odot}} \quad (3)$$

This lies within the range of previously published calibrations ($1 - 3 \times 10^{-10} \text{ M}_{\odot} \text{ yr}^{-1} L_{\odot}^{-1}$). Equation (3) yields SFRs that are 14% lower than the recent calibration of Lehnert & Heckman (1996), and 22% lower than Meurer et al. (1997). The SFR surface density was

then calculated within the radius of the starburst region as determined from the CO maps, or from the infrared maps if high-resolution CO data were not available. The sizes of the regions defined in CO and the infrared show excellent correspondence in cases where comparable resolution data are available (Telesco et al. 1993; Smith & Harvey 1996). Table 2 lists the radii, gas densities, and SFR surface densities derived in this way.

In §4 we analyze the composite properties of the normal disk and starburst samples, so it is important to confirm that the FIR and $H\alpha$ -based SFRs are on a consistent zeropoint. Matching aperture $Br\gamma$ photometry for 18 of the galaxies in our sample is available from the compilations of Puxley, Hawarden, & Mountain (1990), Telesco et al. (1993) and Smith & Harvey (1996), and these allow us to compare the emission-line and FIR SFR scales on a self consistent basis. The FIR-based SFRs were derived using equation (3), while the $Br\gamma$ -based SFRs were derived using equation (2) and a $Br\gamma/H\alpha$ ratio of 0.0103, corresponding to Case B recombination at $T_e = 7500$ K and $N_e = 10^3$ cm⁻⁶ (Osterbrock 1989). No extinction corrections were applied to the $Br\gamma$ data.

Figure 1 shows a comparison of the FIR and $Br\gamma$ -derived SFRs. The solid line shows the correlation expected if the two sets of SFRs were equivalent. The data in Figure 1 closely follow this correlation, but the FIR-derived SFRs are systematically higher by an average of 0.29 ± 0.06 dex, as shown by the dashed line. This displacement could indicate a general inconsistency between the zeropoints of the $H\alpha$ and FIR calibrations of the SFR, which might arise, for example, from errors in the FIR luminosities (many of them extrapolated from the mid-IR), or in the synthesis model that is used to convert the FIR luminosities to SFRs. However there is physical justification for expecting that the $Br\gamma$ fluxes would systematically underestimate the SFRs in many of these objects. The extinction in most regions is so large that one expects part of the ionizing radiation from the starburst to be absorbed by grains, and in some objects extinction of $Br\gamma$ itself is probably significant (e.g., Lutz et al. 1996; Goldader et al. 1997). The $Br\gamma$ -derived SFR will also tend to be systematically lower than the FIR-derived value if the starbursts are observed after the peak of the burst, because the dust heating is dominated by longer lived stars than the emission lines. We provisionally adopt the SFRs from equation (3) in the following analysis, on the tentative assumption that the FIR-based SFRs are more reliable in these objects. However we will also explore the consequences of adopting the lower $Br\gamma$ -based scale, and include this uncertainty in the analysis of the global Schmidt law.

2.3. Uncertainties

Individual uncertainties are not listed for the surface densities listed in Tables 1 and 2, because the predominant errors are systematic in nature and difficult to quantify. However it is important to be aware of nature of these uncertainties and their possible influence on the observed star formation law.

For the normal spiral disks, with SFRs derived from $H\alpha$ luminosities (Table 1), the dominant systematic errors are extinction variations, which introduce a scatter in the SFR densities, and uncertainty in the extrapolated IMF, which could introduce an overall shift in the SFRs (Kennicutt 1983). The dominant errors in the gas densities are variation in the CO/H_2 conversion factor, combined with the limited sampling of the CO measurements in some galaxies (Sage 1993; Young et al. 1995). A realistic estimate for the observational scatter in the SFRs is $\pm 30\text{--}50\%$, or $\pm 0.15\text{--}0.3$ dex (Kennicutt 1983), and the uncertainties in the gas densities are probably comparable. We adopt an average uncertainty of ± 0.2 dex in the following analysis.

The systematic uncertainties in the SFRs and gas densities derived for the starburst galaxies (Table 2) are larger. In many cases the FIR luminosities have been derived from a combination of high-resolution mid-infrared measurements and IRAS FIR fluxes, and there can be substantial uncertainty in the extrapolation to a total FIR flux. In other cases only integrated IRAS fluxes for the galaxies are available, and the presence of significant FIR emission from the region outside of the central starburst will cause the starburst SFR to be systematically overestimated. The SFR will also be overestimated if the dust is heated partly by other sources, such as an active nucleus. Another significant source of uncertainty in the SFRs inferred for individual starbursts is the use of a fixed continuous burst model, though the effect on the overall SFR scale should be lower. The gas densities in the starburst regions are also subject to systematic error as well, mainly through uncertainties in the CO/H_2 conversion factor (e.g., Downes et al. 1993; Solomon et al. 1997). Other smaller sources of uncertainty include the neglect of atomic gas and errors in the radii of the starbursts. The latter errors affect the inferred SFR and gas densities equally, and have less of an effect on the form of the Schmidt law.

The largest of these systematic uncertainties, the L_{FIR} – SFR conversion and the CO/H_2 conversion, could introduce errors in the SFR or gas density scales at the factor of 2 – 3 level (0.3 – 0.5 dex). In our analysis we adopt uncertainties $^{+0.3}_{-0.5}$ dex in both parameters, with the asymmetry reflecting the greater likelihood that the systematic errors tend to lead to overestimates of the SFRs and gas densities. Despite these uncertainties, the data provide very strong constraints on the form of the star formation law, because of the very large range of absolute densities and SFRs represented in the sample, 2 – 6 orders

of magnitude depending on the subsample of interest.

3. RESULTS

3.1. The Schmidt Law in Normal Disks

Figure 2 shows the relationship between the disk-averaged SFR and total gas density (atomic and molecular hydrogen) for the 61 normal spirals in our sample. A clear correlation is apparent in the expected sense of increasing SFR with increasing gas densities, with a mean slope that is considerably steeper than a linear relation (indicated by the dotted and dashed lines). However the scatter in the relation is large, up to a factor of 30 in SFR at a fixed gas density, and comparable to the total range in observed gas density. Consequently the slope of the Schmidt law is poorly constrained. A conventional least squares fit which minimizes (logarithmic) residuals in the SFR density yields $N = 1.29 \pm 0.18$. This slope lies in the middle of the range $N = 0.9 - 1.7$ derived in previous studies with smaller samples (Buat et al. 1989; K89; Buat 1992; Deharveng et al. 1994). A bivariate least squares regression, which takes into account the uncertainties in the gas densities as well, yields a much steeper fit $N = 2.47 \pm 0.39$. Both fits are shown with solid lines in Figure 2. The large difference between these solutions is a direct reflection of the large dispersion in the disk-averaged SFR vs gas density relation, and the result underscores the conclusion that any Schmidt law in these galaxies should be regarded as a *very* approximate parametrization at best.

What is the physical origin of the large dispersion in Figure 2? As discussed earlier, variations in extinction and the CO/H₂ conversion introduce a scatter at about the ± 0.2 dex level in the SFR and gas densities, as signified by the error bars in Figure 2. This can account for roughly half of the observed scatter in the star formation law. The remaining scatter must be real, reflecting a real variation in the mean Schmidt law. Such a variation is not entirely surprising, when one recalls that the local SFRs and gas densities span orders of magnitude within typical disks, and averaging over the entire disk will not necessarily preserve the form of a nonlinear local Schmidt law. The problem is illustrated in Figure 3, which shows the radial SFR vs gas density profiles for 21 of the galaxies in our sample (Paper II). Each profile was produced by measuring the azimuthally averaged gas density and SFR density as a function of galactocentric radius, then plotting the resulting SFR vs gas density relation on a common scale. At high densities the SFRs are well represented by a shallow Schmidt law ($N \sim 1.4$), but the slope of the star formation law steepens abruptly below the threshold density. The disk-averaged SFRs plotted in Figure 2 represent gross averages over these highly nonlinear relations, and the resulting global Schmidt law exhibits

a slope that is intermediate between the $N \sim 1.4$ power-law dependence at high density and the steeper law in the threshold regime. The dispersion in Figure 2 is introduced because the star formation in some galaxies is highly concentrated to the high-density part of the local Schmidt law, while in other systems much of the star formation takes place near the threshold density (see K89). This underscores the caveat that disk-averaged Schmidt law analyzed here contains little physical information about the underlying star formation law. However it does provide a convenient means of parametrizing the gross star formation properties of disks in simple one-zone evolution models. We defer further discussion of the spatially-resolved star formation law for Paper II.

The data in Figure 2 also provide useful information on the average global efficiency of star formation in local disks, the coefficient A in equation (1). The dashed and dotted lines in Figure 2 correspond to constant SFRs per unit gas mass, in units of 1%, 10%, and 100% per 10^8 yr. The choice of 10^8 yr as a fiducial timescale is arbitrary, but it does correspond roughly to a typical orbital time in the disks. The lines are offset by a factor of 1.37 to include helium and heavy elements in the total gas mass. The median efficiency for the disks in Figure 2 is 4.8%, i.e., a typical present-day spiral galaxy converts 4.8% of the gas (within the optical radius) to stars over this period. The efficiencies can be expressed alternatively as gas consumption timescales, with the lines in Figure 2 corresponding to timescales τ_{gas} of 10, 1, and 0.1 Gyr (bottom to top). The median gas consumption time for the disks in this sample is 2.1 Gyr, again referring to the star forming disks alone, and not including corrections for recycling of interstellar gas. Recycling typically extends the actual consumption timescale by factors of 2–3 above the simple calculation (Kennicutt et al. 1994).

Most of the galaxies in Figure 2 possess disk-averaged star formation efficiencies in the range 2 – 10% per 10^8 yr, corresponding to gas consumption times of 1 – 5 Gyr. However several galaxies are more extreme, and the full range of efficiencies is 0.8 – 60% per 10^8 yr ($\tau_{gas} = 0.2 – 12$ Gyr). The shortest timescales correspond to optically-selected starburst galaxies such as NGC 1569 and NGC 3310, while the low extremes are represented by early-type spirals such as M31, NGC 2841, and NGC 4698, where the current SFRs are so low that the future consumption times, even for their modest gas supplies, are comparable to the Hubble time.

Until now our attention has focussed solely on the relationship between the disk-averaged SFR and the total gas density, but we can also examine how the SFRs correlate with the average atomic and molecular gas densities, as shown in Figure 4. These comparisons include galaxies mapped in HI or CO (but not both), so the samples are considerably larger than shown in Figure 2.

The left panel of Figure 4 shows the SFR vs HI density relation for 88 galaxies with H α and HI data in common. The correlation is very reminiscent of the SFR vs total density relation shown in Figure 2, and in fact the correlation coefficients are nearly identical, 0.66 for the SFR – HI relation vs 0.68 for the SFR – HI+H $_2$ relation. This is not entirely surprising, as HI accounts for approximately half of the total gas density on average. These results are consistent with previous analyses based on smaller samples by K89, Buat (1992), Deharveng et al. (1994), Boselli (1994), and Boselli et al. (1995). The physical interpretation of the SFR vs HI Schmidt law is not obvious, however. It may trace the physical influence of the atomic gas density on the SFR, but it could be that the SFR regulates the density of HI, through the photodissociation of molecular gas by hot stars (Shaya & Federman 1987; Tilanus & Allen 1989).

The correlation between the H α -based SFRs and H $_2$ density is much weaker, as shown in the right panel of Figure 4. This has been reported previously, and appears to hold independently of whether SFRs based on H α , UV continuum fluxes, or FIR fluxes are analyzed (Buat 1992; Boselli 1994). Such a poor correlation between the SFR and molecular gas densities is unexpected, and it has led some to suggest that variations in the CO/H $_2$ conversion factor are responsible for the scatter (K89; Boselli 1994; Boselli et al. 1995). Our data provide indirect support for this interpretation. Several lines of evidence suggest that the Galactic CO/H $_2$ conversion factor is valid in regions with near-solar metallicity, but that it tends to systematically underestimate the H $_2$ mass in metal-poor regions, such as are found in the outer disks of spirals or in low-luminosity galaxies (e.g., Maloney & Black 1988; Kenney & Young 1988; Rubio et al. 1993; Wilson 1995). To test whether this effect might be contributing to the scatter in Figure 4, we subdivided our sample by blue luminosity, with solid points denoting galaxies with $L_B > 10^{10} L_\odot$ ($M_B < -19.5$ for $H_0 = 75$ km s $^{-1}$ Mpc $^{-1}$) and open circles representing fainter galaxies. The mean metal abundance in disks is well correlated with luminosity, so this provides an approximate separation of the galaxies by abundance, around a value of $\sim 1 Z_\odot$ (Zaritsky, Kennicutt, & Huchra 1994). Figure 4 shows that the luminous, metal-rich spirals do show a much better defined SFR vs H $_2$ density correlation, comparable in slope and scatter to the correlations with total and HI density. By contrast, the low-luminosity galaxies show essentially no correlation between the SFR and CO-inferred H $_2$ densities, with many CO-weak galaxies showing unusually *high* SFRs. Although this is hardly a conclusive result, it offers circumstantial evidence that variations in the CO/H $_2$ conversion factor are responsible for most of the scatter in the SFR vs molecular gas density relation. Our conclusions are consistent with those of Boselli (1994) and Boselli et al. (1995), and the reader is referred to those papers for more detailed discussions of this problem.

3.2. The Schmidt Law in Circumnuclear Starbursts

We can perform a parallel analysis for the infrared-selected starbursts, and the results are summarized in Figure 5. The comparison is directly analogous to that shown for the normal disks in Figure 2, except that the SFRs are derived from FIR luminosities, and the SFRs are correlated with the H_2 gas density alone (the disks are expected to be overwhelmingly molecular, as discussed earlier). The SFRs and densities are averaged within the radii of the central molecular disks and starbursts, which have typical dimensions of order 1 kpc. The error bars indicate the typical uncertainties, as discussed in §2.3.

The starburst galaxies also show a well-defined Schmidt law, in this case with a best fitting least squares slope $N = 1.40 \pm 0.13$ (bivariate regression) or $N = 1.28 \pm 0.08$ (errors in SFRs only). The Schmidt law is better defined than for the normal disks, but partly because there is a much larger dynamic range in SFR and gas densities in the starburst sample; the dispersion in absolute SFR per per unit area at fixed gas density is only slightly lower in the starburst sample. Star formation threshold effects are probably unimportant in the starburst disks, and this might also account for the somewhat tighter Schmidt law among these objects.

Although the starburst disks exhibit a SFR vs gas density relation that is qualitatively similar in form to that seen in the normal spiral disks, the physical regime we are probing is radically different. The average gas surface densities here range from 10^2 to $10^5 \text{ M}_\odot \text{ pc}^{-2}$, compared to a typical range of order $1 - 100 \text{ M}_\odot \text{ pc}^{-2}$ in normal disks (Figures 2, 3). The mean densities of the starburst disks are comparable instead to those of individual molecular cloud complexes in normal galaxies. For example, the largest HII/GMC complexes in M31, M33, and M51 have molecular masses and sizes corresponding to mean surface densities of $40 - 500 \text{ M}_\odot \text{ pc}^{-2}$ (Wilson & Rudolph 1993; Wilson & Scoville 1992; Nakai & Kuno 1995). This is comparable to the *low end* of the density range for the starbursts in Figure 5. The mean densities of some of the starbursts approach those of Galactic molecular cloud cores, but extending over kiloparsec diameter regions. The star formation densities are just as extraordinary. For example, the central 10 pc core of the 30 Doradus giant HII region contains $\sim 10^4 \text{ M}_\odot$ in young stars, which corresponds to $\Sigma_{SFR} \sim 100 \text{ M}_\odot \text{ yr}^{-1} \text{ kpc}^{-2}$ if the star formation timescale is as short as 10^6 yr ; the average SFR density averaged over the entire HII region is $\sim 1 - 10 \text{ M}_\odot \text{ yr}^{-1} \text{ kpc}^{-2}$. Thus the regions we are studying have projected SFRs per unit area that approach the maximum limit observed in nearby optically-selected star clusters and associations (Meurer et al. 1997), but extending over regions up to a kiloparsec in radius.

Not surprisingly, the global star formation efficiencies in the starburst sample are much higher than in the normal disk sample (e.g., Young et al. 1986; Solomon & Sage 1988;

Sanders, Scoville, & Soifer 1991). In Figure 5 we show the same lines of constant star formation efficiency and gas consumption times as in Figure 2 (1%, 10%, and 100% per 10^8 yr). The median rate of gas consumption is 30% per 10^8 yr, 6 times larger than for the normal disk samples, and the efficiencies reach 100% per 10^8 yr for the most extreme objects. It is interesting to note that the shortest gas consumption times are comparable to the dynamical timescales of the parent galaxies, implying that the most luminous starbursts are forming stars near the limit set by the gas accumulation timescale (Lehnert & Heckman 1996).

4. THE COMPOSITE SCHMIDT LAW

Taken together, the normal disk and starburst samples span a dynamic range of approximately 10^5 in gas surface density and over 10^6 in SFR per unit area. Figure 6 shows the composite relation, with the normal spirals shown as solid circles and the starbursts as solid squares. Quite remarkably, the data are consistent with a common Schmidt law extending over the entire density range.

Figure 6 shows that the normal disk and starburst samples occupy completely separate regimes in gas density and SFR per unit area, not a surprising result given the very different selection criteria for the two samples. But before we interpret the composite relation it is important to establish whether there is a smooth physical continuity between the normal disk and starburst regimes, and to confirm the consistency of the $H\alpha$ and FIR-derived SFR scales. To this end we derived $H\alpha$ -based SFRs and gas densities for the central regions of 25 of the normal spirals in Table 1 ($R < 25''$), using our $H\alpha$ images and published HI and CO maps (Paper II). The resulting SFR and gas densities are shown as open circles in Figure 6. These regions span the physical parameter space between the normal disks as a whole and the infrared-selected circumnuclear starburst regions. Figure 6 shows that the gas densities and $H\alpha$ -derived SFRs of these regions fall on the composite Schmidt law defined by the normal disk and starburst samples, and fill the transition region between the two physical regimes. The same conclusion can be drawn by comparing the SFRs of the infrared-selected starburst galaxies in Figure 5 with the spatially-resolved SFRs of the normal disks shown in Figure 3; the starbursts lie on the extrapolation of the high-density star formation laws observed in the spiral disks. This result, combined with the $Br\gamma$ -FIR comparison discussed earlier, gives us confidence that we are measuring the form of the star formation law on a self-consistent basis across the sample.

The solid line in Figure 6 shows a bivariate least-square fit to the composite relation defined by the normal disks and the starbursts (but not including the open circles). In this

case we applied equal weights to all of the data points, in order to avoid having the fit driven by the normal spirals in the lower left region of Figure 6. This yields a best fitting index $N = 1.40 \pm 0.05$ (bivariate regression) or $N = 1.35 \pm 0.03$ (errors in SFRs only). These are nearly identical to the Schmidt law fits for the starburst sample alone, which further confirms the consistency of the large-scale star formation laws in the two samples.

The formal uncertainties listed here assume random errors of ± 0.3 dex in the SFRs and gas densities, but it underestimates the full uncertainty in the Schmidt law, because we have not accounted for the possibility of a systematic shift in the overall SFR or density scales for the starburst sample as a whole. The effect of such a shift is easily calculated. For example, reducing the SFRs for all of the starbursts by a factor of two, to match the Br γ calibration in Figure 1, would lower the best fitting index N from 1.40 to 1.28. Likewise, lowering the gas masses in the starbursts by a factor of two, to take into account the possibility that the CO/H $_2$ conversion factor is systematically lower, would *increase* N by approximately the same amount, from 1.4 to 1.5. This range of values provides a fairer estimate of the actual uncertainty in the composite Schmidt law. Folding together all of these uncertainties, we adopt as our final result:

$$\Sigma_{SFR} = (2.5 \pm 0.7) \times 10^{-4} \left(\frac{\Sigma_{gas}}{1 M_{\odot} \text{ pc}^{-2}} \right)^{1.4 \pm 0.15} M_{\odot} \text{ yr}^{-1} \text{ kpc}^{-2}. \quad (4)$$

Figure 6 shows that equation (4) provides an excellent parametrization of the global SFR, over a density range extending from the most gas-poor spiral disks to the cores of the most luminous starburst galaxies. This may account for why conventional galaxy evolution models, which usually are based on a Schmidt law parametrization of the SFR, often produce realistic predictions of the gross star formation properties of galaxies.

There are limitations to the Schmidt law in equation (4) that should be borne in mind, however, when applying this recipe to galaxy evolution models or numerical simulations. Although the full range of SFRs and gas densities are very well represented by a single power law with $N \simeq 1.4$, the scatter in SFRs about the mean relation is substantial, ± 0.3 dex rms, and individual galaxies deviate by as much as a factor of 7. Consequently equation (4) provides at most a statistical description of the global SFR, averaged over large samples of galaxies. Another potential limitation for its application to simulations and models is the need to accurately specify the linear sizes of the relevant star forming regions. This is relatively straightforward for normal disks, where the scaling radius is comparable to the photometric radius of the galaxy or the edge of the active star forming disk. It may be more difficult to model in starbursts, however, where the intense star formation is usually concentrated in a region that is a few percent of the radius of the parent galaxy. Fortunately the slope of the Schmidt law is relatively shallow, and a modest error in the scaling radius

will displace the inferred SFR and gas densities nearly along a line of slope $N = 1$, nearly parallel to the Schmidt law itself. This is illustrated in Figure 6, where a short diagonal line shows the effect of changing the scaling radius by a factor of two (for a fixed gas mass and total SFR).

5. DISCUSSION: INTERPRETATION AND OTHER RECIPES

The Schmidt law in Figure 6 is so well defined that it is tempting to identify a simple, unique physical origin for the relation. However we find that a Schmidt law is not the only simple parametrization that can reproduce the range of SFRs observed in this sample, and this serves as a caution against overinterpreting the physical nature of the empirical star formation law. In this section we briefly discuss the form of the Schmidt law expected from simple gravitational arguments, and demonstrate that a simple kinematical model provides an equally useful recipe for modelling the large-scale SFR.

Numerous theoretical scenarios which produce a Schmidt law with $N = 1 - 2$ can be found in the literature (Larson 1992 and references therein). Simple self-gravitational models for disks can reproduce the large-scale star formation thresholds observed in galaxies (Quirk 1972; K89), and the same basic model is consistent with a Schmidt law at high densities with index $N \sim 1.5$ (Larson 1988, 1992). For example in a simple self-gravitational picture in which the large-scale SFR is presumed to scale with the growth rate of perturbations in the gas disk, the SFR will scale as the gas density divided by the growth timescale:

$$\rho_{SFR} \propto \frac{\rho_{gas}}{(G\rho_{gas})^{-0.5}} \propto \rho_{gas}^{1.5}. \quad (5)$$

where ρ_{gas} and ρ_{SFR} are the volume densities of gas and star formation. The corresponding scaling of the projected surface densities will depend on the scale height distribution of the gas, with $N = 1.5$ expected for a constant mean scale height, a reasonable approximation for the galaxies and starbursts considered here. Although this is hardly a robust derivation, it does show that a global Schmidt law with $N \sim 1.5$ is physically plausible.

In a variant of this argument, Silk (1997) has suggested a generic form of the star formation law, in which the SFR surface density scales with the ratio of the gas density to the local dynamical timescale:

$$\Sigma_{SFR} \propto \frac{\Sigma_{gas}}{\tau_{dyn}} \propto \Sigma_{gas} \Omega_{gas} \quad (6)$$

where τ_{dyn} refers in this case to the local orbital timescale of the disk, and Ω is the angular

rotation speed. Models of this general class have been studied previously by Wyse (1986) and Wyse & Silk (1989), though with different scalings of the gas density and separate treatment of the atomic and molecular gas. Equation (6) might be expected to hold if, for example, star formation triggering by spiral arms or bars were important, in which case the SFR would scale with orbital frequency. To test this idea, we compiled rotation velocities for the galaxies in Tables 1 and 2, and used them to derive a characteristic value of τ_{dyn} for each disk. The timescale τ_{dyn} was defined arbitrarily as $2\pi R/V(R) = 2\pi/\Omega(R)$, the orbit time at the outer radius R of the star forming region. The mean orbit time in the star forming disk is smaller than τ_{dyn} defined in this way, by a factor of 1 – 2, depending on the form of the rotation curve and the radial distribution of gas in the disk. We chose to define τ_{dyn} and Ω at the outer edge of the disk to avoid these complications. Tables 1 and 2 list the adopted values, in units of 10^8 yr. Face-on galaxies or those with poorly determined (rotational) velocity fields were excluded from the analysis.

Figure 7 shows the relationship between the observed SFR density and Σ_{gas}/τ_{dyn} for our sample. The solid line is not a fit but simply a line of slope unity which bisects the relation for normal disks. This alternate prescription for the star formation law provides a surprisingly good fit to the data, both in terms of the slope and the relatively small scatter about the mean relation. When compared over the entire density range the observed law is slightly shallower than predicted by equation (7) (slope ~ 0.9 instead of 1); on the other hand the fit to the normal disk sample is as tight as a Schmidt law. The zeropoint of the line corresponds to a SFR of 21% of the gas mass per orbit at the outer edge of the disk. Since the average orbit time within the star forming disk is about half that at the disk edge, this implies a simple parametrization of the local star formation law:

$$\Sigma_{SFR} \simeq 0.017 \Sigma_{gas} \Omega_{gas}, \quad (7)$$

in other words the SFR is $\sim 10\%$ of the available gas mass per orbit.

From a strictly empirical point of view, the Schmidt law in equation (4) and the kinematical law in equation (7) offer two equally valid parametrizations for the global SFRs in galaxies, and either can be employed as a recipe in models and numerical simulations. It is unclear whether the kinematic model can fit the radial distribution of star formation as well as a Schmidt law, and we plan to explore this in Paper II.

The two parametrizations also offer two distinct interpretations of the observation that the star formation efficiency in central starbursts is much higher than found in quiescent star forming disks (e.g., Young et al. 1986; Solomon & Sage 1988; Sanders et al. 1991). In the Schmidt law picture, the higher efficiencies in starbursts are simply a consequence of their much higher gas densities. For a given index N , the SFR per unit gas mass will scale

as $\Sigma_{gas}^{(N-1)}$, and hence for the law observed here roughly as $\Sigma_{gas}^{0.4}$. The central starbursts have characteristic gas densities that are 100 – 10000 times higher than the average for normal disks, hence we would expect the global star formation efficiencies to be 6 – 40 times higher, as observed. In the alternative picture in which the SFR is presumed to scale with Σ_{gas}/τ_{dyn} , the high SFRs and star formation efficiencies in starburst galaxies simply reflect the smaller physical scales and shorter dynamical timescales in these compact central regions. It is difficult to differentiate between these alternatives with disk-averaged measurements alone, and since the global star formation law is mainly useful as an empirical parametrization, the distinction may not be important. Deeper insight into the physical nature of the star formation law requires spatially resolved data for individual disks, of the kind that will be analyzed in Paper II.

Several individuals contributed to the large set of H α data analyzed in this paper, and it is a pleasure to thank them. The KPNO data used in this paper were obtained as part of other projects in collaboration with R. Braun, R. Walterbos, and P. Hodge. C. Martin worked on the reduction of the spatially resolved H α data shown in Figure 3. I am also grateful to J. Black, J. Ostriker, S. Sakai, P. Solomon, S. White, and especially J. Silk for comments and suggestions about early versions of this work. I am also grateful to the anonymous referee for several comments that improved the paper. Some of the data used in this paper were obtained on the 2.3m Bok telescope at Steward Observatory. This research was supported by the National Science Foundation through grant AST-9421145.

REFERENCES

- Aalto, S., Booth, R.S., Black, J.H., Koribalski, B., & Wielebinski, R. 1994, *A&A*, 286, 365
- Armus, L., Heckman, T., & Miley, G. 1989, *ApJ*, 347, 727
- Ball, R., Sargent, A.I., Scoville, N.Z., Lo, K.Y., & Scott, S.L. 1985, *ApJ*, 298, L21
- Becklin, E.E., Gatley, I., Matthews, K., Neugebauer, G., Sellgren, K., & Werner, M.W. 1980, *ApJ*, 236, 441
- Bernlöhr, K. 1993, *A&A*, 270, 20
- Bohlin, R.C., Savage, B.D., & Drake, J.F. 1978, *ApJ*, 224, 132
- Boselli, A. 1994, *A&A*, 292, 1
- Boselli, A., Gavazzi, G., Lequeux, J., Buat, V., Casoli, F., Dickey, J., & Donas, J. 1995, *A&A*, 300, L13
- Bosma, A. 1978, Ph.D. thesis, University of Groningen
- Bosma, A., Goss, W.M., & Allen, R.J. 1981, *A&A*, 93, 106
- Braun, R., Walterbos, R.A.M., Kennicutt, R.C., & Tacconi, L.J. 1994, *ApJ*, 420, 558
- Broeils, A.H., & van Woerden, H. 1994, *A&AS*, 107, 129
- Buat, V., Deharveng, J.M., & Donas, J. 1989, *A&A*, 223, 42
- Buat, V. 1992, *A&A*, 264, 444
- Caplan, J., & Deharveng, L. 1986, *A&A*, 155, 297
- Casertano, S., & van Gorkom, J.H. 1991, *AJ*, 101, 1231
- Casoli, F., Combes, F., Dupraz, C., Gerin, M., Encrenaz, P., Salez, M. 1988, *A&A*, 192, 17
- Casoli, F., Dupraz, C., Combes, F., & Kazes, I. 1991, *A&A*, 251, 1
- Deharveng, J.M., Sasseen, T.P., Buat, V., Bowyer, S., Lampton, M., & Wu, X. 1994, *A&A*, 289, 715
- Devereux, N.A., Kenney, J.D.P., & Young, J.S. 1992, *AJ*, 103, 784
- de Vaucouleurs, G., de Vaucouleurs, A., & Corwin, H.G. 1986, *Second Reference Catalog of Bright Galaxies* (Austin: Univ. Texas Press) (RC2)
- Downes, D., Solomon, P.M., & Radford, S.J.E. 1993, *ApJ*, 414, 13
- Downes, D., Reynaud, D., Solomon, P.M., & Radford, S.J.E. 1996, *ApJ*, 461, 186
- Dupraz, C., Casoli, F., Combes, F., & Kazes, I. 1991, *A&A*, 228, 5
- Engelbracht, C.W. 1997, Ph.D. thesis, University of Arizona

- Fall, S.M., & Efstathiou, G.P. 1980, MNRAS, 193, 189
- Garcia-Barreto, J.A., Downes, D., Combes, F., Gerin, M., Magri, C., Carrasco, L., & Cruz-Gonzalez, I. 1991, A&A, 244, 257
- Goldader, J.D., Joseph, R.D., Doyon, R., & Sanders, D.B. 1997, ApJ, 474, 104
- Hunter, D.A., Gillett, F.C., Gallagher, J.S., Rice, W.L., & Low, F.J. 1986, ApJ, 303, 171
- Ishiguro, M. et al. 1989, ApJ, 344, 763
- Israel, F.P., & van Driel, W. 1990, A&A, 236, 323
- Jackson, J.M., Eckart, A., Cameron, M., Wild, W., Ho, P.T.P., Pogge, R.W., & Harris, A.I. 1991, ApJ, 375, 105
- Kenney, J.D.P., & Young, J.S. 1988, ApJ, 326, 588
- Kenney, J.D.P., Wilson, C.D., Scoville, N.Z., Devereux, N.A., & Young, J.S. 1992, ApJ, 395, L79
- Kenney, J.D.P., Carlstrom, J.E., & Young, J.S. 1993, ApJ, 418, 687
- Kennicutt, R.C. 1983, ApJ, 272, 54
- Kennicutt, R.C. 1989, ApJ, 344, 685
- Kennicutt, R.C. 1992, ApJ, 388, 310
- Kennicutt, R.C. 1997, in Gas Disks in Galaxies, ed. J.M. van der Hulst (Dordrecht: Kluwer), in press
- Kennicutt, R.C., & Kent, S.M. 1983, AJ, 88, 1094
- Kennicutt, R.C., & Chu, Y.-H. 1988, AJ, 95, 720
- Kennicutt, R.C., Edgar, B.K., & Hodge, P.W. 1989, ApJ, 337, 761
- Kennicutt, R.C., Tamblyn, P., & Congdon, C.W. 1994, ApJ, 435, 22
- Knapen, J.H. 1997, MNRAS, 286, 403
- Koper, E. 1993, Ph.D. thesis, University of Leiden
- Larson, R.B. 1988, in Galactic and Extragalactic Star Formation, ed. R.E. Pudritz & M. Fich (Dordrecht: Kluwer), 435
- Larson, R.B. 1992, in Star Formation in Stellar Systems, ed. G. Tenorio-Tagle, M. Prieto, & F. Sánchez (Cambridge: Cambridge Univ. Press), 125
- Lehnert, M., & Heckman, T. 1996, ApJ, 472, 546
- Leitherer, C., & Heckman, T.M. 1995, ApJS, 96, 9
- Lo, K.Y. et al. 1984, ApJ, 282, L59

- Lo, K.Y., Cheung, K.W., Masson, C.R., Phillips, T.G., Scott, S.L., & Woody, D.R. 1987, *ApJ*, 312, 574
- Lonsdale, C.J., & Helou, G. 1987, *ApJ*, 314, 513
- Lutz, D. et al. 1996, *A&A*, 315, 137
- Maloney, P., & Black, J. 1988, *ApJ*, 325, 389
- Martin, C.L., & Kennicutt, R.C. 1998, in preparation (Paper II)
- Mauersberger, R., Henkel, C., Wielebinski, R., Wiklind, T., & Reuter, M.P. 1996, *A&A*, 305, 221
- Meurer, G.R., Heckman, T.M., Lehnert, M.D., Leitherer, C., & Lowenthal, J. 1997, *AJ*, 114, 54
- Mulder, P.S., van Driel, W., & Braine, J. 1995, *A&A*, 300, 687
- Nakai, N., & Kuno, N. 1995, *PASJ*, 47, 761
- Navarro, J., & Steinmetz, M. 1997, *ApJ*, 478, 13
- Osterbrock, D.E. 1989, *The Astrophysics of Gaseous Nebulae and Active Galactic Nuclei* (Mill Valley: University Science Books), 84
- Puxley, P.J., Hawarden, T.G., & Mountain, C.M. 1990, *ApJ*, 364, 77
- Quirk, W.J. 1972, *ApJ*, 176, L9
- Rhee, M.-H., & van Albada, T.S. 1996, *A&AS*, 115, 407
- Rickard, L.J., & Harvey, P.M. 1983, *ApJ*, 268, L7
- Rogstad, D.H., Lockhart, I.A., & Wright, M.C.H. 1974, *ApJ*, 193, 309
- Rogstad, D.H., Shostak, G.S., & Rots, A.H. 1973, *A&A*, 22, 111
- Romanishin, W. 1990, *AJ*, 100, 373
- Rots, A.H. 1980, *A&AS*, 41, 189
- Rubio, M., Lequeux, J., & Boulanger, F. 1993, *A&A*, 271, 9
- Sage, L.J. 1993, *A&AS*, 100, 537
- Sanders, D.B., & Mirabel, I.F. 1996, *ARA&A*, 34, 749
- Sanders, D.B., Scoville, N.Z., & Soifer, B.T. 1991, *ApJ*, 370, 158
- Schmidt, M. 1959, *ApJ*, 129, 243
- Scoville, N., Hibbard, J.E., Yun, M.S., & van Gorkom, J.H. 1994, in *Mass-Transfer Induced Activity in Galaxies*, ed. I. Shlosman (Cambridge: Cambridge Univ. Press), 191

- Shaya, E.J., & Federman, S.R. 1987, *ApJ*, 319, 76
- Silk, J. 1997, *ApJ*, in press
- Smith, B.J., & Harvey, P.M. 1996, *ApJ*, 468, 139
- Solomon, P.M., Downes, D., Radford, S.J.E., & Barrett, J.W. 1997, *ApJ*, 478, 144
- Solomon, P.M., & Sage, L. 1988, *ApJ*, 334, 613
- Telesco, C.M., & Harper, D.A. 1980, *ApJ*, 235, 392
- Telesco, C.M., Dressel, L.L., & Wolstencroft, R.D. 1993, *ApJ*, 414, 120
- Tilanus, R.P.J., & Allen, R.J. 1989, *ApJ*, 339, L57
- van der Kruit, P.C., & Shostak, G.S. 1982, *A&A*, 105, 359
- van der Kruit, P.C., & Shostak, G.S. 1984, *A&A*, 134, 258
- van Moorsel, G.A. 1983, *A&AS*, 54, 19
- Veilleux, S., Kim, D.-C., Sanders, D.B., Mazzarella, J.M., & Soifer, B.T. 1995, *ApJS*, 98, 171
- Walterbos, R.A.M. 1988, in *Galactic and Extragalactic Star Formation*, ed. R. Pudritz & M. Fich (Dordrecht: Kluwer), 361
- Walterbos, R.A.M., & Greenawalt, B. 1996, *ApJ*, 460, 696
- Wang, Z., Schweizer, F., & Scoville, N.Z. 1992, *ApJ*, 396, 510
- Warmels, R.H. 1986, Ph.D. thesis, University of Groningen
- Warmels, R.H. 1988, *A&AS*, 72, 427
- Wevers, B.M.H.R., van der Kruit, P.C., & Allen, R.J. 1986, *A&AS*, 66, 502
- Wild, W., Harris, A.I., Eckart, A., Genzel, R., Graf, U.U., Jackson, J.M., Russell, A.P.G., & Stutzki, J. 1992, *A&A*, 265, 447
- Wilson, C.D. 1995, *ApJ*, 448, L97
- Wilson, C.D., & Rudolph, A.L. 1993, *ApJ*, 406, 477
- Wilson, C.D., & Scoville, N. 1992, *ApJ*, 385, 512
- Wyse, R.F.G. 1986, *ApJ*, 311, L41
- Wyse, R.F.G., & Silk, J. 1987, *ApJ*, 339, 700
- Young, J.S., Schloerb, F.P., Kenney, J.D.P., & Lord, S. 1986, *ApJ*, 304, 443
- Young, J.S., Xie, S., Kenney, J.D.P., & Rice, W.L. 1989, *ApJS*, 70, 699
- Young, J.S. et al. 1995, *ApJS*, 98, 219

Young, J.S., Kenney, J.D.P., Lesser, A., & Rownd, B. 1996, AJ, 112, 1903

Figure Captions

FIG. 1.— A comparison of integrated SFRs derived from Br γ emission-line fluxes and far-infrared continuum luminosities, for 18 infrared-selected starburst galaxies. The solid line shows the relation expected from eqs. (2) and (3). The dashed line is the best fitting mean relation.

FIG. 2.— Relation between the disk-averaged SFR per unit area and gas density for 61 normal disk galaxies. The solid lines are least square fits to the Schmidt law, as described in the text. The dashed and dotted lines correspond to constant global star formation efficiencies and gas consumption timescales, as indicated.

FIG. 3.— Profiles of the azimuthally averaged SFR per unit area as a function of gas density for 21 spirals with spatially resolved H α data.

FIG. 4.— Correlation of the disk-averaged SFR per unit area with the average surface densities of HI (left) and H $_2$ (right). The H $_2$ densities were derived using a constant CO/H $_2$ conversion factor. In the right panel, solid circles denote galaxies with $L_B > 10^{10} L_\odot$, while open circles denote galaxies with $L_B < 10^{10} L_\odot$.

FIG. 5.— Relation between the disk-averaged SFR per unit area and molecular gas density for 36 infrared-selected circumnuclear starbursts. The solid line shows a bivariate least squares fit to the Schmidt law, as described in the text. The dashed and dotted lines correspond to constant global star formation efficiencies and gas consumption timescales, as indicated.

FIG. 6.— Composite star formation law for the normal disk (solid circles) and starburst (squares) samples. Open circles show the SFRs and gas densities for the centers of the normal disk galaxies. The line is a least squares fit with index $N = 1.40$. The diagonal short line shows the effect of changing the scaling radius by a factor of two.

FIG. 7.— Relation between the SFR for the normal disk and starburst samples and the ratio of the gas density to the disk orbital timescale, as described in the text. The symbols are the same as in Figure 6. The line is a median fit to the normal disk sample, with the slope fixed at unity as predicted by equation (7).

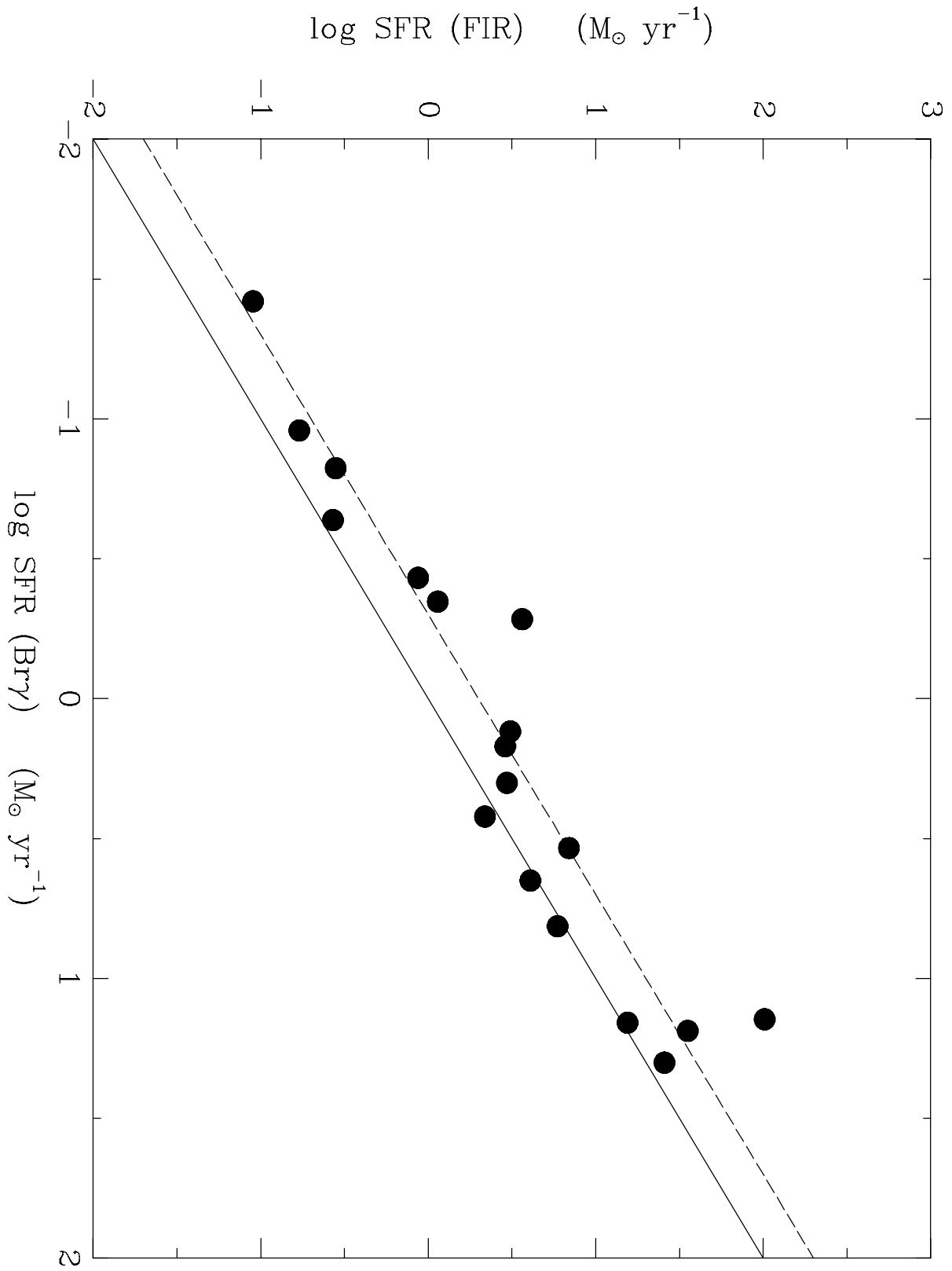


TABLE 1
NORMAL SPIRALS

NGC	D (")	$\log \Sigma_{HI}^a$	$\log \Sigma_{H_2}^a$	$\log \Sigma_{gas}^a$	$\log \Sigma_{SFR}^b$	τ_{dyn}^c	References
224	165.2	0.66	-0.58	0.68	-3.13	4.6	1,5,22
598	55.9	1.02	-0.71	1.03	-2.47	4.0	2,6,23
628	10.2	0.77	0.41	0.93	-2.18	...	3,4,7,24,25
772	7.2	0.60	0.68	0.94	-2.84	7.9	5,8,26
925	8.9	0.85	0.05	0.91	-2.44	7.3	2,4,7,25
1058	3.0	0.51	0.38	0.75	-2.20	...	4,9,24
1569	2.5	1.30	0.10	1.33	-0.80	2.0	3,10,24
2336	6.9	0.75	0.40	0.91	-1.92	7.4	2,11,24
2403	15.8	0.86	-0.46	0.88	-2.15	3.5	3,7,27
2841	6.8	0.31	0.86	0.97	-2.99	1.6	3,12,27
2903	10.7	0.55	0.57	0.86	-2.31	3.1	3,4,7,25
2976	4.9	0.72	0.63	0.98	-1.66	1.3	2,4,13,24,26
3031	22.2	0.82	-0.46	0.85	-2.50	2.7	4,6,27
3310	3.5	1.08	0.27	1.14	-1.14	2.5	3,14,24,26
3338	5.9	0.75	-0.06	0.81	-2.56	4.0	2,8,26
3368	6.5	0.66	0.59	0.93	-2.55	2.7	3,4,6,24
3486	7.1	0.85	-0.20	0.88	-2.46	3.2	4,13,24
3521	8.1	0.70	1.07	1.22	-1.91	3.3	3,4,15,24,25
3631	4.6	0.65	1.00	1.16	-1.73	4.9	2,16,24,25
3675	5.9	0.50	0.83	0.99	-2.01	2.2	2,13,25,26
3726	5.4	0.89	0.59	1.06	-2.28	3.2	2,7,26
3893	3.9	0.86	0.63	1.06	-1.96	3.0	3,13,26
3938	5.3	0.77	1.00	1.20	-2.11	...	2,17,24
4178	4.0	1.10	-0.22	1.13	-2.27	3.9	2,6,24
4189	2.3	0.78	0.85	1.12	-2.09	...	2,6,24
4254	5.2	0.88	1.23	1.39	-1.70	3.5	3,6,24
4258	15.1	0.49	-0.10	0.59	-2.36	4.8	3,4,7,27
4294	2.5	0.95	0.17	1.02	-1.87	3.0	3,6,24
4299	1.7	1.06	0.33	1.13	-1.53	...	3,6,24
4303	5.9	0.78	1.01	1.21	-1.74	4.8	3,6,24
4321	6.8	0.56	1.06	1.14	-2.07	4.5	3,6,24
4394	3.9	0.15	0.46	0.63	-2.88	3.2	3,6,24,27
4402	3.1	0.28	1.01	1.08	-2.80	4.2	3,6,27
4501	6.0	0.44	0.98	1.09	-2.21	3.3	3,6,24,27
4519	3.1	0.97	0.33	0.99	-1.98	2.9	2,6,25
4535	6.3	0.61	0.79	1.01	-2.38	5.2	3,6,24
4548	5.1	0.21	0.51	0.69	-2.52	3.4	3,6,24,27
4561	1.4	1.37	0.98	1.52	-1.93	1.6	2,6,24
4569	7.9	-0.41	0.57	0.61	-2.78	5.0	3,6,24,27
4571	3.7	0.41	0.63	0.83	-2.56	4.7	3,6,24
4579	5.1	0.04	0.73	0.81	-2.32	2.8	3,6,24,27
4639	2.7	0.59	0.18	0.73	-2.11	2.2	3,6,27
4647	3.4	0.45	0.91	1.04	-2.22	3.5	3,6,26
4651	3.5	0.84	0.66	1.06	-1.98	2.7	3,6,24,26
4654	4.3	0.80	0.80	1.10	-2.06	3.5	3,6,24,26
4689	3.9	0.18	0.86	0.94	-2.38	3.2	3,6,24,27
4698	3.7	-0.13	0.01	0.25	-3.55	2.5	3,6,27
4713	2.6	0.97	0.22	1.04	-1.53	3.2	3,6,24,26

TABLE 1—*Continued*

NGC	D (')	$\log \Sigma_{HI}^a$	$\log \Sigma_{H_2}^a$	$\log \Sigma_{gas}^a$	$\log \Sigma_{SFR}^b$	τ_{dyn}^c	References
4736	10.5	0.28	0.41	0.65	-2.22	2.7	3,4,12,24
4826	8.0	-0.40	0.64	0.67	-2.47	...	2,4,18,24
5033	9.1	0.73	0.49	0.93	-2.64	7.7	3,7,24
5055	11.0	0.68	1.00	1.17	-2.32	3.8	3,4,7,24
5194	10.0	0.76	1.38	1.47	-1.78	3.4	3,4,7,24,27
5236	11.0	0.88	1.63	1.70	-1.41	2.8	3,19,27
5457	26.9	1.01	0.22	1.09	-2.46	8.8	3,20,27
6207	2.6	0.95	0.25	1.03	-1.70	2.6	3,8,24
6217	3.0	0.73	1.16	1.29	-1.91	2.9	2,6,24
6503	4.9	0.61	0.53	0.89	-2.08	1.7	3,4,7,24
6643	3.4	0.85	0.77	1.11	-1.81	3.7	3,8,24,26
6946	10.7	0.94	1.04	1.30	-1.88	3.5	3,4,21,24,25
7331	8.5	0.67	0.87	1.08	-2.33	5.8	3,12,25,27

^aUnits $M_{\odot} \text{ pc}^{-2}$

^bUnits $M_{\odot} \text{ yr}^{-1} \text{ kpc}^{-2}$

^cUnits 10^8 yr

REFERENCES.—

CO Data Sources:

(1) Koper 1993; (2) Young et al. 1995; (3) Young et al. 1989; (4) Sage 1993;

HI Data Sources:

(5) Koper 1993; (6) Warmels 1986; (7) Wevers et al. 1986; (8) Rhee & van Albada 1996; (9) van der Kruit & Shostak 1984; (10) Israel & van Driel 1990; (11) van Moorsel 1983; (12) Bosma 1978; (13) Broeils & van Woerden 1994; (14) Mulder et al. 1995; (15) Casertano & van Gorkom 1991; (16) Knapen 1997; (17) van der Kruit & Shostak 1982; (18) Braun et al. 1994; (19) Rogstad et al. 1973; (20) Bosma et al. 1981; (21) Rogstad et al. 1974;

H α Data Sources:

(22) Walterbos 1988; (23) Kennicutt et al. 1989; (24) Kennicutt & Kent 1983; (25) Young et al. 1996; (26) Romanishin 1990; (27) This paper.

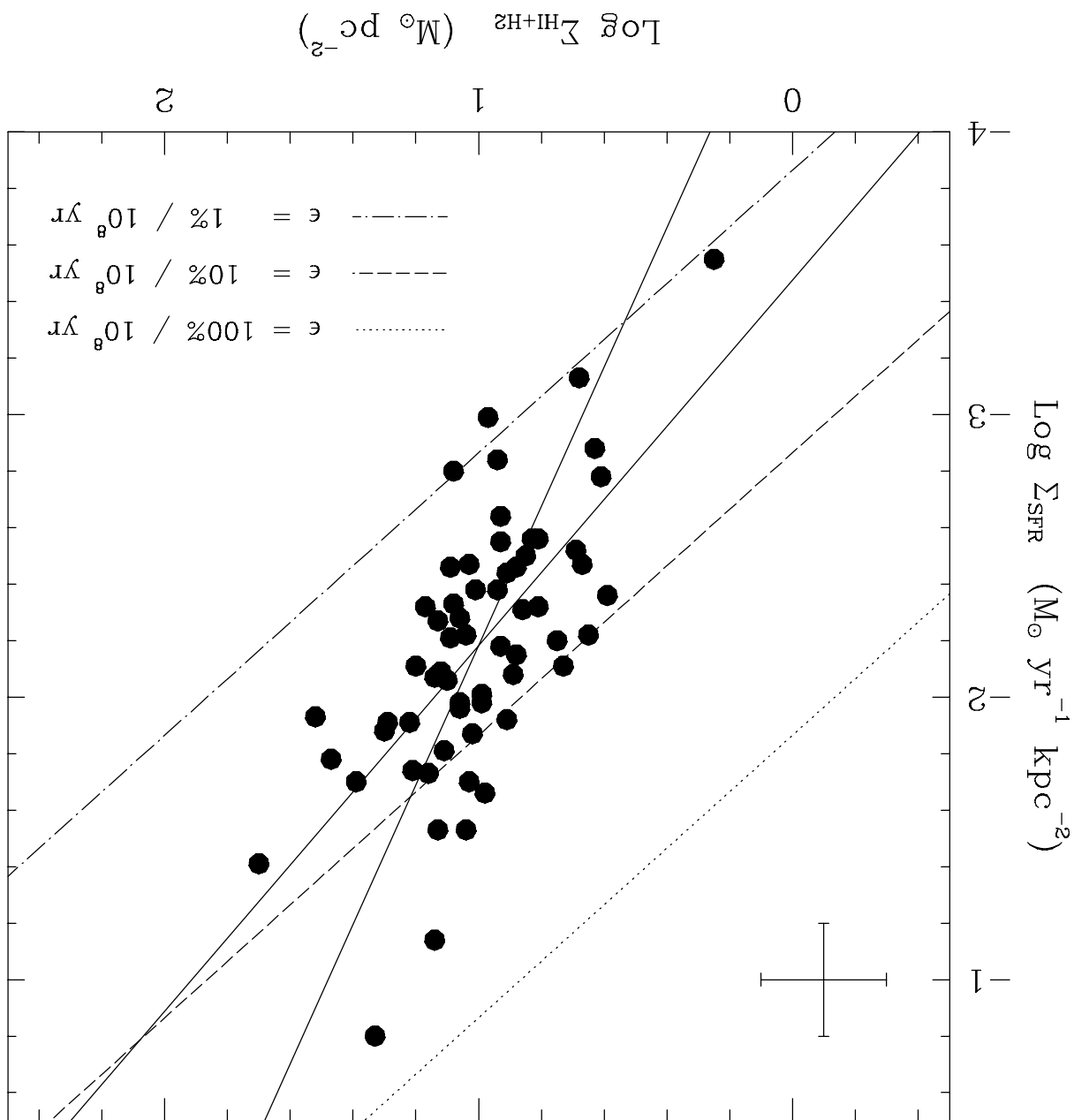


TABLE 2
INFRARED-SELECTED CIRCUMNUCLEAR STARBURSTS

Name	D (")	$\log \Sigma_{H_2}^a$	$\log \Sigma_{SFR}^b$	τ_{dyn}^c	References
NGC 253	24	3.35	1.24	0.15	1,2,3
NGC 520	5	3.81	1.32	...	4
NGC 660	31	2.60	0.06	0.46	1
NGC 828	5	3.66	1.10	0.26	3
NGC 891	35	2.61	-0.58	0.22	1
NGC 1097	35	2.67	-0.20	0.29	1,2
NGC 1614	4	3.72	1.79	0.19	3
NGC 1808	30	2.65	0.08	0.52	1,2
NGC 2146	17	2.83	0.84	0.32	1
NGC 2623	8	2.87	1.00	...	5
NGC 2903	8	2.60	-0.11 ^d	...	6
NGC 3034	29	3.52	1.48	0.09	7,8
NGC 3079	5	4.25	1.63	...	3
NGC 3256		3.13	0.68	1.22	9
NGC 3351	14	2.83	0.24 ^e	0.13	10,11
NGC 3504	16	2.90	0.11 ^e	0.20	12
NGC 3627	39	2.28	-0.77	0.38	1
NGC 3690	24	2.28	-0.10	...	1
NGC 4736	24	2.25	-0.18	0.14	1
NGC 5194	54	2.49	-1.11	0.44	1
NGC 5236	22	2.87	0.30	0.21	1,2
NGC 6240	3	4.11	1.87	0.24	3
NGC 6946	27	2.26	-0.30	0.94	1,2,6,13,14
NGC 7252	11	2.61	-0.08	...	15,16
NGC 7552	22	2.38	0.16	...	1
IC 342	67	2.06	-0.41	...	17,18
IC 694	2.6	4.10	2.40	...	3
IC 883	3.4	3.95	1.54	0.23	3
IC 1623	3.6	3.81	1.67	0.24	3
Maffei 2	40	2.46	-0.27	0.78	2,19,20
Arp 55	8	2.73	0.32	1.34	3
Arp 220	2	4.76	2.98	0.06	3
IR 10173+0828	7	2.41	0.48	1.68	3
IR 17208-0014	3	4.09	2.01	...	3
VII Zw 31	5	3.11	0.82	1.18	3
ZW 049.057	3	3.90	1.77	0.19	3

^aUnits $M_{\odot} \text{ pc}^{-2}$

^bUnits $M_{\odot} \text{ yr}^{-1} \text{ kpc}^{-2}$

^cUnits 10^8 yr , for $H_0 = 75 \text{ km s}^{-1} \text{ Mpc}^{-1}$

^dSFR based on $\text{Br}\gamma$ luminosity

^eSFR based on FIR and $\text{Br}\gamma$ luminosities

REFERENCES.— (1) Smith & Harvey 1996; (2) Telesco et al. 1993; (3) Mauersberger et al. 1996; (4) Scoville et al. 1994; (5) Casoli et al. 1988; (6) Jackson et al. 1991; (7) Lo et al. 1987; (8) Wild et al. 1992; (9) Casoli et al. 1991; (10) Kenney et al. 1992; (11) Devereux et al. 1992; (12) Kenney et al. 1993; (13) Ball et al. 1985; (14) Telesco & Harper 1980; (15) Dupraz et al. 1990; (16) Wang et al. 1992; (17) Lo et al. 1984; (18) Becklin et al. 1980; (19) Ishiguro et al. 1989; (20) Rickard & Harvey 1983.

